iScience

CellPress
OPEN ACCESS

Article

Enhanced visible-light-driven photocatalytic activity in SiPGaS/arsenene-based van der Waals heterostructures

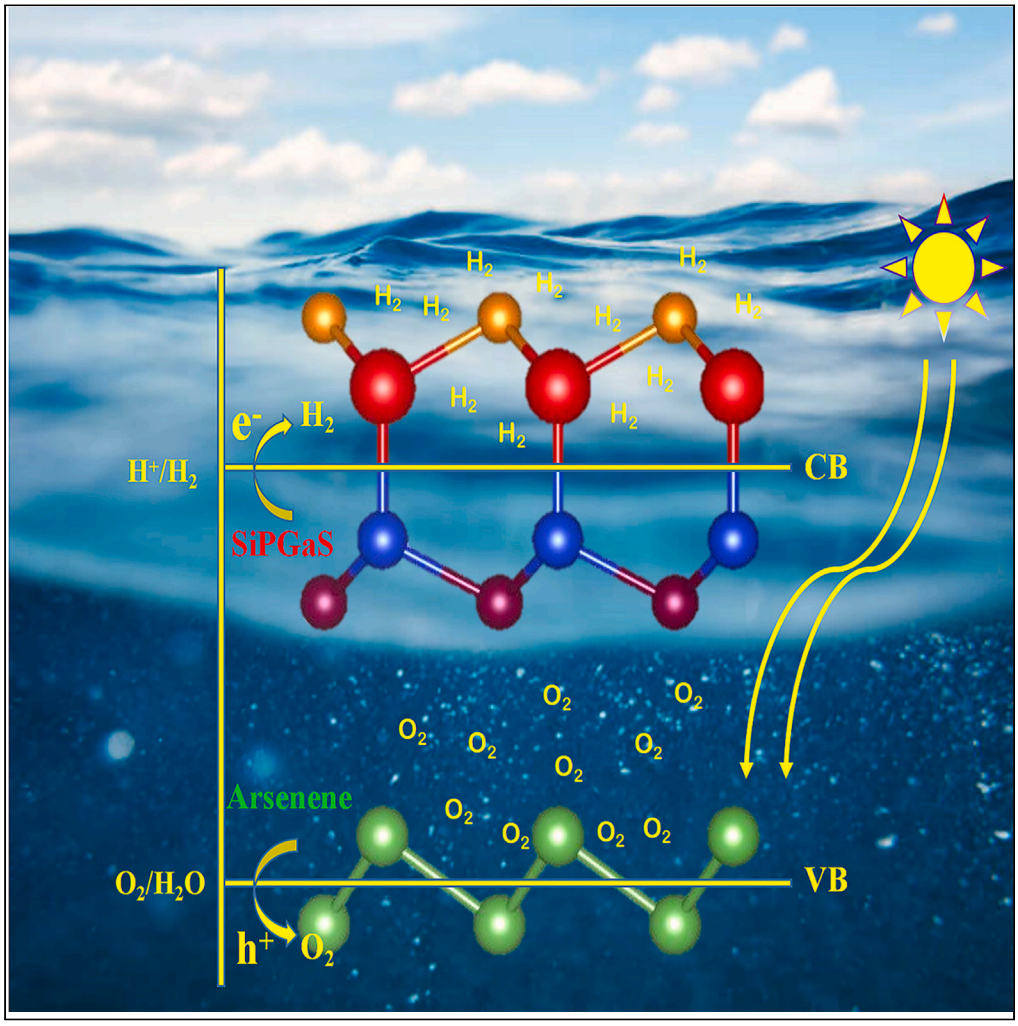

Anwar Ali, Ismail Shahid, Iqtidar Ahmad, Bin Lu, Haitao Zhang, Wen Zhang, Ping Kwan Johnny Wong

zhang.wen@nwpu.edu.cn (W.Z.)
pingkwanj.wong@nwpu.edu.cn (P.K.J.W.)

Highlights

GaSSiP/arsenene and SiPGaS/arsenene heterostructures are predicted from first principles

Heterostructures are promising photocatalysts for water splitting

An increased interlayer distance improves photocatalysis at pH = 2

The transition from type-II to type-III band alignment occurs at 8% compressive strain

Ali et al., iScience *26*, 108025
October 20, 2023
https://doi.org/10.1016/j.isci.2023.108025

iScience

CellPress
OPEN ACCESS

Article

Enhanced visible-light-driven photocatalytic activity in SiPGaS/arsenene-based van der Waals heterostructures

Anwar Ali,[1,2] Ismail Shahid,[4] Iqtidar Ahmad,[5] Bin Lu,[1,2,3] Haitao Zhang,[1,2] Wen Zhang,[1,2,*] and Ping Kwan Johnny Wong[1,2,3,6,*]

SUMMARY

Van der Waals heterostructures (vdWHs) showcase robust and tunable light-matter interactions, establishing an intriguing realm for investigating atomic-scale photocatalytic properties. Here, we employ *ab initio* methods to study the photocatalytic and optical properties of semiconducting SiPGaS/arsenene-based vdWHs with a type-II band alignment. Across the heterointerfaces, there exists significant built-in electric fields and large potential drop, in turn facilitating the spatial separation of photo-generated electron-hole pairs. These vdWHs further possess high carrier mobility in the order of 10^2 $cm^2V^{-1}S^{-1}$, which combining with appropriate band edge positions, endow the vdWHs an absorption coefficient of $\sim 10^5$ cm^{-1} to harvest a maximal portion of the solar spectrum for visible-light-driven photocatalytic applications. Our findings also reveal transition of the type-II band alignment in a type-III configuration via compressive strain for tunneling field-effect transistor application. Furthermore, both types of vdWHs exhibit enhanced suitability for photocatalysis under conditions with a pH of 2.

INTRODUCTION

Advancing renewable and clean energy sources stand as a foundational approach to fulfill the escalating energy needs and confront the environmental challenges arising from the excessive utilization of fossil fuels.[1] Among the most promising alternatives is the conversion of solar energy into hydrogen (H_2) and oxygen (O_2) through a process of water splitting. This process gains momentum with the use of semiconductor-based photocatalysts.[2–5] To create a comprehensive water-splitting photocatalyst, two crucial criteria must be fulfilled: (1) the electronic band gap must exceed 1.23 eV and (2) the positions of the band edges should align with the oxidation potential of O_2/H_2O (−5.67 eV) and the reduction potential of H^+/H_2 (−4.44 eV) within the water molecule.[6] Additionally, to bolster water splitting efficiency, a high absorption coefficient (preferably within the visible range), high charge carrier mobility, and effective conversion of solar energy are crucial parameters to be met.[7] Two-dimensional (2D) layered materials have garnered extensive research attention due to their wide-ranging applications, including photocatalysis,[8,9] optoelectronics,[10–13] and spintronics.[14–17] However, these materials encounter inherent limitations, such as pronounced excitonic effects and large effective mass, which contribute to the rapid recombination of photoexcited charge carriers.[18] The performance of devices is notably hindered by the short lifetime of these charge carriers, leading to a considerable reduction in quantum efficiency.[18,19] To surmount these inherent challenges, various strategies have been explored, including strain engineering,[20] electric fields,[21] and van der Waals heterostructures (vdWHs),[22,23] among others. Among these approaches, the construction of vdWHs stands out as one of the most promising techniques for enhancing optoelectronic and photocatalytic efficiency, owing to its practicality and effectiveness in spatially separating electron-hole pairs.[23] Typically, vdWHs exhibit superior photocatalytic and optical properties when compared to individual constituent layers.[24,25] For instance, heterostructures such as $WS_2/MoSe_2$,[26] $MoTe_2$/BAs,[27] g-C_3N_4/SiPGaS,[28] and boron phosphide-blue phosphorene[29] have demonstrated improved optoelectronic and photocatalytic performances theoretically, surpassing their respective single-layer counterparts.

Based on their band alignment, vdWHs can be categorized into three primary types: type-I (straddling gap), type-II (staggered gap), and type-III (broken gap).[30,31] Each of these categories possesses distinct attributes that render them advantageous for various electronic devices. The type-I band alignment proves favorable for light-emitting diodes and semiconductor lasers, as it spatially confines electrons and holes, thereby facilitating efficient recombination.[32] Conversely, the type-II band alignment, characterized by a substantial band offset, enables

[1]ARTIST Lab for Artificial Electronic Materials & Technologies, School of Microelectronics, Northwestern Polytechnical University, Xi'an 710072, Shaanxi, P.R. China
[2]Yangtze River Delta Research Institute of Northwestern Polytechnical University, Taicang 215400, P.R. China
[3]NPU Chongqing Technology Innovation Center, Chongqing 400000, P.R. China
[4]School of Materials Science and Engineering, Institute of New Energy Material Chemistry, Renewable Energy Conversion and Storage Centre (ReCast), Key Laboratory of Advanced Energy Materials Chemistry (Ministry of Education), Nankai University, Tianjin 300350, P.R. China
[5]College of Materials Science and Engineering, Shenzhen University, Shenzhen 518060, P.R. China
[6]Lead contact
*Correspondence: zhang.wen@nwpu.edu.cn (W.Z.), pingkwanj.wong@nwpu.edu.cn (P.K.J.W.)
https://doi.org/10.1016/j.isci.2023.108025

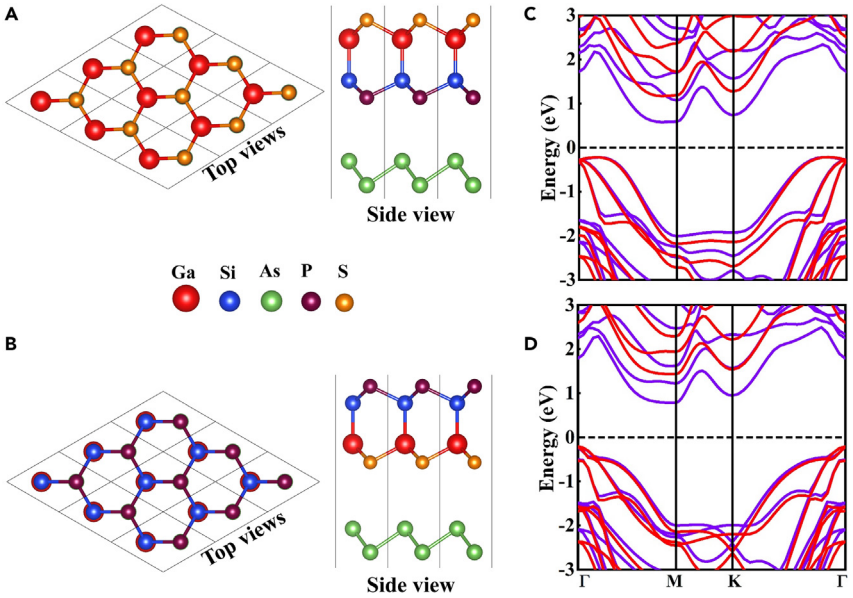

Figure 1. Atomic and electronic band structures

(A) Top and side views of atomic structure of GaSSiP/arsenene vdWH.

(B) Top and side views of atomic structure of SiPGaS/arsenene vdWH.

(C) Electronic band structure of GaSSiP/arsenene vdWH (violet/red solid energy band line present the PBE/HSE06 functional result).

(D) Electronic band structure of SiPGaS/arsenene vdWH (violet/red solid energy band line present the PBE/HSE06 functional result).

efficient carrier separation, making it well-suited for photovoltaic and photocatalytic devices.[33,34] The band offset of the type-III alignment contributes to engineering the transition energy from the conduction to the valence band, rendering it suitable for designing tunneling field-effect transistors (t-FETs) and wavelength photodetectors.[33]

Recent research has spotlighted the exceptional electronic and photocatalytic characteristics of single-layer SiPGaS[28,35] and arsenene.[36,37] Among the group V-IV-III-VI (IV = Si, Ge, Sn; V = N, P; III = Al, Ga, In; VI = O, S),[35] single-layer SiPGaS has been chosen as a representative due to the successful exfoliation of the single-layer GaS from bulk crystals[38] and its substantial responsiveness to visible light. This characteristic enhancement in optical properties serves to improve the overall performance of vdWHs.[28] On the other hand, arsenene exhibits puckered and buckled structures with indirect band gaps. The latter structure, being slightly more stable than the former,[39] maintains a reasonable band gap of 1.6 eV and demonstrates excellent absorption of visible and UV light.[36,37] This renders arsenene a suitable candidate for constructing vdWHs with efficient optical and photocatalytic capabilities.[40] Moreover, the calculated lattice mismatch between single-layer arsenene and SiPGaS is less than 5%, which proves conducive to heterostructuring. Building upon these earlier findings, the objective of this study is to ascertain whether SiPGaS and arsenene can form stable vdWHs while retaining their exceptional electronic and photocatalytic characteristics.

In this study, we have conducted a comprehensive analysis of the electronic structure, charge transfer phenomena, optical properties, and photocatalytic efficiency of SiPGaS/arsenene-based vdWHs. We have furthermore explored how these properties can be modulated by strain and interlayer spacing. The SiPGaS/arsenene-based vdWHs exhibit a staggered band gap and generate robust built-in electric fields across the heterointerface, thereby effectively separating photogenerated electron-hole pairs. Notably, through the expansion of the interlayer spacing, both types of vdWHs become suitable for photocatalytic processes at a pH of 2. Moreover, the application of an 8% compressive strain induces a transition from a type-II to a type-III band alignment, rendering these vdWHs potential candidates for tunneling field-effect transistor application.

RESULTS AND DISCUSSION

Atomic structures and stabilities

The atomic configurations of single-layer SiPGaS and arsenene are presented in Figures S1A and S1B (supplemental information). The calculated in-plane lattice parameter for single-layer SiPGaS is 3.53 Å, while that of single-layer arsenene is 3.57 Å. These values are consistent with prior studies.[28,40–42] To achieve an atomic registry, a matching ratio of 1:1 is considered for the unit cells of single-layer arsenene and SiPGaS. We estimated the lattice mismatch (δ) between the single-layers as ~1%, using the formula $\delta = |a_{arsenene} - a_{SiPGaS}|/a_{arsenene}$, where a_{SiPGaS} and $a_{arsenene}$ are the relaxed lattice parameters of single-layer SiPGaS and arsenene respectively. To construct vdWHs, single-layer SiPGaS is placed vertically over arsenene, as depicted in Figures 1A and 1B. Employing the relaxed geometries, three possible stacking configurations were established, as shown in Figures S2A and S2B. Notably, both S- and P-terminated surfaces of single-layer SiPGaS can create vdWHs with arsenene. This has led us to define two distinct models in our calculations, as illustrated in Figures 1A and 1B. In the subsequent context, the

CellPress
OPEN ACCESS

Table 1. Binding energy E_i (eV) for different stacking (i = 1, 2, 3), interlayer distance d_o (Å), in-plane lattice constants a (Å), work functions Φ (eV) band gaps E_g (eV) using PBE and HSE06 methods for GaSSiP/arsenene SiPGaS/arsenene vdWHs

Heterostructures	GaSSiP/arsenene	SiPGaS/arsenene
E_1	−1.58	−1.54
d_o	3.64	3.75
E_2	−1.49	−1.48
d_o	3.71	3.72
E_3	−1.57	−1.53
d_o	3.61	3.76
Φ	5.54	5.68
a	3.55	3.55
CBM	−4.35	−4.27
VBM	−5.72	−5.93
E_g (PBE)	0.79	1.00
E_g (HSE)	1.37	1.65

Conduction band minimum (CBM) and valence band maximum (VBM) band edges of the vdWHs.

SiPGaS/arsenene model corresponds to the S-termination facing the arsenene surface, whereas the GaSSiP/arsenene model features the P-terminated surface of single-layer SiPGaS facing that of arsenene.

To quantitatively assess the stability in terms of energy for the different stacking configurations, the binding energies of the vdWHs are defined as $E_b = E_{SiPGaS/arsenene} - E_{SiPGaS} - E_{arsenene}$. Here, $E_{SiPGaS/arsenene}$ is the total energy of the vdWHs, while $E_{arsenene}$ and E_{SiPGaS} represent the energies of the individual single-layer arsenene and SiPGaS, respectively. The optimized lattice parameters (a), binding energies (E_b), and interlayer distances (d_0) of the various stacking arrangements for both GaSSiP/arsenene and SiPGaS/arsenene vdWHs are summarized in Table 1. It is important to note that a negative E_b indicates an energetically stable system, and a lower value of E_b suggests a more stable configuration. Among all possible stackings, stacking-1 for both vdWHs has the smallest E_b, suggesting higher stability. As a result, further calculations were conducted using the most stable stacking-1 configuration. To evaluate dynamical stability, we computed their phonon dispersion spectra as well as their corresponding single-layers. As depicted in Figures 2A–2D, neither the single-layers nor their vdWHs exhibit imaginary frequencies in their phonon dispersion spectra, affirming their dynamical stability. To verify their thermal stability, the results of ab initio molecular dynamics (AIMD) simulations for the vdWHs were displayed in Figures 2E and 2F. These figures illustrate that the free energy fluctuations are minimal and no significant geometric distortions occur even after heating at 500 K for 5 ps, indicating their robust thermal stability.

Electronic properties

To gain insights into the electronic properties of GaSSiP/arsenene and SiPGaS/arsenene vdWHs, we begin by examining the electronic band gaps of the individual single-layers, as shown in Figures S1C and S1D. Both single-layers emerge as indirect band gap semiconductors, with band gap values of 1.85 eV and 2.60 eV by the PBE functional, and 1.62 eV and 2.26 eV within the HSE06 functional, respectively. These values are in line with previous findings.[28,40–42] Moving to Figures 1C and 1D, the band structures of the vdWHs are depicted. Notably, the GaSSiP/arsenene vdWH exhibits an indirect band gap character, with the valence band maximum (VBM) positioned at the Γ-M points and the conduction band minimum (CBM) at the M point. On the other hand, the SiPGaS/arsenene vdWH has its VBM at Γ and CBM at the M point. According to the PBE functional, the GaSSiP/arsenene and SiPGaS/arsenene vdWHs exhibit predicted band gap values of 0.79 eV and 1.00 eV, respectively. More accurate HSE06 computations result in band gap values of 1.37 eV for GaSSiP/arsenene and 1.65 eV for SiPGaS/arsenene. Projected band structures (Figures 3A and 3B) reveal that the CBM and VBM stem from the individual single-layers SiPGaS and arsenene, respectively, for both types of vdWHs. This arrangement gives rise to a type-II band alignment, which is further corroborated by the partial density of states (PDOS) in Figures 3C and 3D, where the CBM and VBM of the vdWHs are seen to predominantly originate from the P-p and As-p orbitals of single-layers SiPGaS and arsenene, respectively. To elucidate the type-II band alignment, schematic maps of the three types of semiconductor vdWHs and the contact mechanism before and after constructing the vdWHs are provided in Figures 3E and 3F. This band alignment causes photoexcited holes on the SiPGaS side to migrate toward the VBM of arsenene due to the valence band offset. Similarly, the conduction band offset at the heterointerface propels photoexcited electrons on the arsenene side to move toward the CBM of the SiPGaS layer. This type-II band alignment suggests the SiPGaS/arsenene-based vdWHs as an efficient photocatalyst.[43]

Interfacial properties

To investigate the interlayer charge transfer and subsequent built-in electric field at the interfacial region, we plotted the charge density difference ($\Delta\rho$) for GaSSiP/arsenene and SiPGaS/arsenene vdWHs, as depicted in Figure 4. The difference in charge density difference is

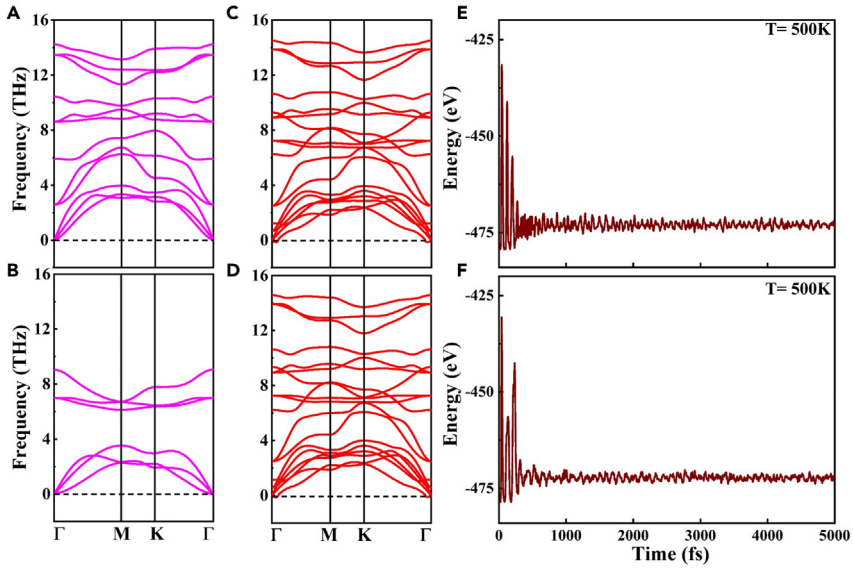

Figure 2. Phonon band structures and AIMD plots

(A) Phonon band structure of single-layer SiPGaS.
(B) Phonon band structure of single-layer arsenene.
(C) Phonon band structure of GaSSiP/arsenene vdWH.
(D) Phonon band structure of SiPGaS/arsenene vdWH.
(E) AIMD plot of GaSSiP/arsenene vdWH.
(F) AIMD plot of SiPGaS/arsenene vdWH.

calculated using the equation $\Delta\rho = \rho_{SiPGaS/arsenene} - \rho_{SiPGaS} - \rho_{arsenene}$, where $\rho_{SiPGaS/arsenene}$, $\rho_{arsenene}$ and ρ_{SiPGaS} are the electron densities of the vdWHs, the parent single-layers arsenene and SiPGaS, respectively. The yellow and cyan regions in Figures 4A and 4B represent regions of charge depletion and accumulation, respectively. Due to electron transfer from arsenene to SiPGaS, a hole-rich region is formed. On the other hand, the transferred electrons accumulate on the SiPGaS surface, giving rise to an electron-rich zone. This combination establishes a built-in electric field that reduces the recombination rate of photoexcited electron-hole pairs, extending their lifetime. The sizes of the built-in electric fields for GaSSiP/arsenene and SiPGaS/arsenene vdWHs are 1.37 and 1.14 eVÅ^{-1}, respectively. Here, we compare the calculated work function (WF) of single-layers SiPGaS and arsenene, in order to verify the charge transfer mechanism. The WF of the system can be expressed as: $\Phi = E_{vac} - E_F$, where Φ denotes WF, E_F is the Fermi level and E_{vac} is the vacuum level. We find that the WF of single-layer SiPGaS is 6.59 eV, larger than that of arsenene (5.64 eV). Accordingly, this causes electron transfer from arsenene to SiPGaS through their interface until a dynamic equilibrium is established.[44] The electrostatic potentials of both vdWHs are displayed in Figures 4C and 4D. We observe a large potential drop (ΔV) of 4.82 and 4.63 eV across the interface of GaSSiP/arsenene and SiPGaS/arsenene vdWHs, respectively. Notably, these potential drops values exceed those of other photocatalysts, such as blue phosphorene/BSe (ΔV = 1.40 eV),[45] blue phosphorene/C_2N (ΔV = 1.04 eV),[46] ZnO/CdS (ΔV = 3.73 eV),[47] GaAs/SiH (ΔV = 0.844 eV)[48] and C_2N/ZnSe (ΔV = 0.844 eV).[49] The large potential drop between the arsenene and SiPGaS layers indicates a robust built-in electric field at the interface, which boost the photogenerated carrier separation in type-II heterostructures.[19]

Carrier mobility

Carrier mobility (μ) stands as an important figure of merit for a photocatalyst. For example, a high carrier mobility would cause photogenerated electrons and holes to move quickly to the catalyst's surface and promote photocatalytic activity. The mobility of carriers in 2D materials can be expressed using the deformation potential theory.[50]

$$\mu_{2D} = \frac{2e\hbar^3 C_{2D}}{3K_B T|m^*|^2 E_{DP}^2} \quad \text{(Equation 1)}$$

Where T is temperature (equal to 300 K here), e is the electronic charge, $\hbar$ is the reduced Planck's constant and K_B denote the Boltzmann constant. The effective mass m^* is defined as $m^* = \hbar^2(\partial E^2(k)/\partial k^2)^{-1}$, where k and $E(k)$ are the wave vector and its associated energy. C_{2D} is the elastic modulus of the material determined by $C_{2D} = 1/S_0(\partial^2 E_{total}/\partial\varepsilon^2)$, where S_0 denotes area of the unstrained system, E_{total} is the total energy, and ε is the uniaxial strain. The deformation potential constant E_{DP} is obtained by $E_{DP} = \partial E_{edge}/\partial\varepsilon$, which indicates a shift in the band edges due to strain. The obtained values of E_{DP}, C_{2D}, m^* and μ_{2D} of the single-layers and their heterostructures are summarized in

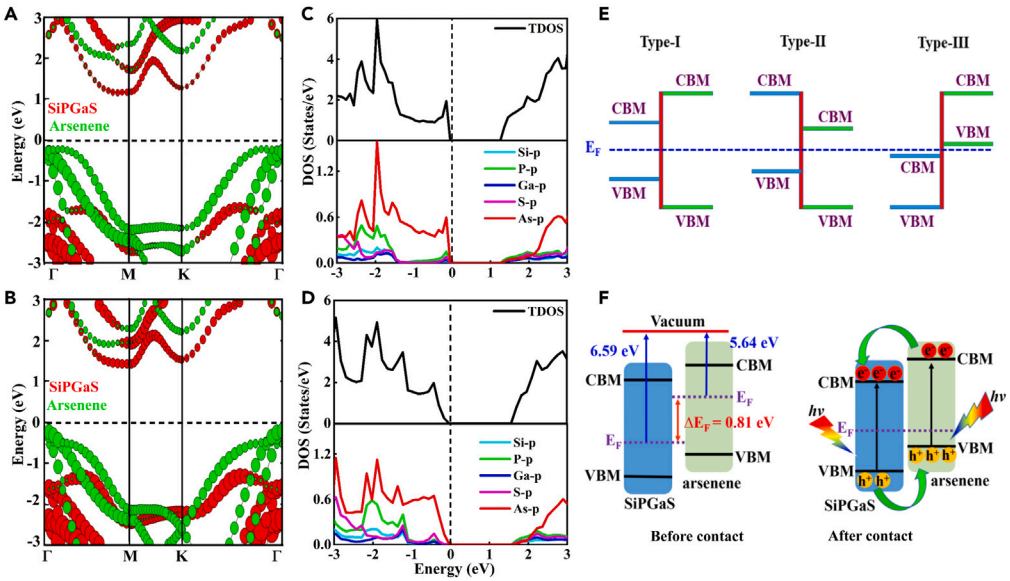

Figure 3. Calculated projected band structures, density of states and band alignments using the HSE06 method

(A) Projected band structure of GaSSiP/arsenene vdWH.

(B) Projected band structure of SiPGaS/arsenene vdWH.

(C) Density of states of GaSSiP/arsenene vdWH.

(D) Density of states of SiPGaS/arsenene vdWH.

(E) Schematic diagram of three kinds of semiconductor vdWH.

(F) Schematic diagram of type-II band alignment before and after constructing the vdWH.

Table 2. The mobility of the electron is a slightly higher compared to that of the hole. Remarkably, high carrier mobilities of 3.20×10^2 and 4.44×10^2 $cm^2V^{-1}S^{-1}$ are achieved for GaSSiP/arsenene and SiPGaS/arsenene vdWHs, respectively.

Photocatalytic and optical properties

Photocatalytic hydrogen generation has emerged as a highly promising way for solar energy conversion. To achieve efficient water splitting, it is crucial that the positions of the conduction band edge (CBE) and valence band edge (VBE) of a photocatalyst straddle the redox potentials of water. These potentials exhibit significant pH-dependent variations. At pH = 0, the standard redox potential for water reduction (H^+/H_2) is −4.44 eV, while it is −5.67 eV for water oxidation (O_2/H_2O).[9] In both GaSSiP/arsenene and SiPGaS/arsenene vdWHs, the oxidation reaction occurs on the arsenene layer due to the photoinduced holes present on this layer, while the reduction reaction takes place on the SiPGaS layer due to the photogenerated electrons present on this layer. Figure 5 illustrates the CBE and VBE positions of both GaSSiP/arsenene and SiPGaS/arsenene vdWHs, as well as their individual single-layers, with respect to the redox potentials of water at pH = 0. The calculated band edge positions of SiPGaS/arsenene-based vdWHs with respect to the redox potentials of water are found to be more favorable for water splitting compared to other photocatalysts reported in the literature, such as GeC/Al_2SO,[51] Blue Phosphorus/$Mg(OH)_2$,[52] and ZnO/BSe.[53] The single-layers arsenene and SiPGaS are active photocatalysts. However, the CBE of arsenene and VBE of SiPGaS are located far from the reduction and oxidation potentials, making both single-layers weak photocatalytic materials. Compared to individual layers, the GaSSiP/arsenene and SiPGaS/arsenene vdWHs can effectively separate photoinduced charge carriers, and their band edges are located at more favorable positions, enhancing their photocatalytic performance.

Water splitting photocatalysts generally exhibit an ability to effectively capture a substantial portion of solar energy radiation, owing to their suitable band alignment and band gap characteristics. Categorizing the potential applications of materials in optical devices necessitates a thorough understanding of their optical properties.[54] Here, we have examined the imaginary $\varepsilon_2(\omega)$ part of the dielectric function and absorption coefficients $\alpha(\omega)$ of individual layers and their GaSSiP/arsenene and SiPGaS/arsenene vdWHs. Figure 6A reveals several peaks in the energy range from 0 to 6 eV, due to electron transitions from the occupied states to the unoccupied states of the parent single-layers and their vdWHs. The single-layer arsenene shows multiple peaks in the range of 2.2–6 eV, while the single-layer SiPGaS only displays peaks in the ultraviolet energy range. This suggests the ability of these single-layers to absorb solar energy in their specific energy ranges, considering the energy distribution of the solar spectrum to be approximately 52% infrared (IR), 43% visible and 5% ultraviolet (UV).[55] Compared to their parent single-layers, the calculations indicate that the vdWHs have significant absorption peaks that effectively capture both visible and ultraviolet regions of solar spectrum. These findings suggest that these vdWHs have the potential to capture a significant portion of solar energy, possibly up to 50%. Furthermore, the absorption coefficients $\alpha(\omega)$ of both single-layers and their GaSSiP/arsenene and

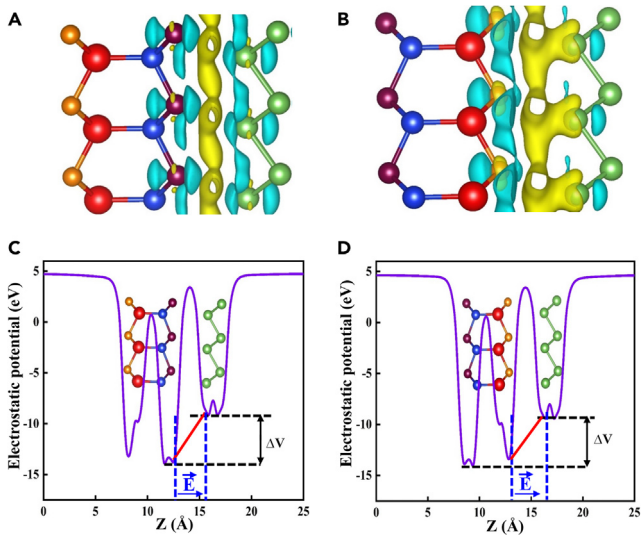

Figure 4. Calculated charge density difference and electrostatic potential using the HSE06 method

(A) Charge density difference plot of GaSSiP/arsenene vdWH.

(B) Charge density difference plot of SiPGaS/arsenene vdWH.

(C) Electrostatic potential of GaSSiP/arsenene vdWH.

(D) Electrostatic potential of SiPGaS/arsenene vdWH.

SiPGaS/arsenene vdWHs are graphically presented in Figure 6B. The optical absorption coefficient $\alpha(\omega)$ is influenced by the dispersion of light intensity that decreases over a specific distance in the medium. Remarkably, both the GaSSiP/arsenene and SiPGaS/arsenene vdWHs have demonstrated impressive absorption coefficients up to 10^5 cm^{-1} in the visible and ultraviolet energy ranges. Based on these findings, we predict the vdWHs to have potential applications in photovoltaic and photocatalytic devices.

To investigate the water-splitting efficiency of SiPGaS/arsenene-based vdWHs, we have computed the solar-to-hydrogen efficiency (η_{sth}). Here, the η_{sth} can be determined by $\eta_{sth} = \eta_{abs} \times \eta_{cu}$,[27] where the parameters η_{abs} and η_{cu} represent the efficiency of light absorption and carrier utilization, respectively. Moreover, the η_{abs} is calculated by:

$$\eta_{abs} = \frac{\int_{E_g}^{\infty} P(\hbar\omega)d(\hbar\omega)}{\int_{0}^{\infty} P(\hbar\omega)d(\hbar\omega)} \quad \text{(Equation 2)}$$

where the parameters $P(\hbar\omega)$ and E_g signify the AM1.5G solar flux at photon energy $\hbar\omega$ and the electronic bandgap of the SiPGaS/arsenene-based vdWHs, respectively. The η_{cu} is expressed as:

$$\eta_{cu} = \frac{\Delta G \int_{E}^{\infty} \frac{P(\hbar\omega)}{\hbar\omega} d(\hbar\omega)}{\int_{E_g}^{\infty} P(\hbar\omega)d(\hbar\omega)} \quad \text{(Equation 3)}$$

where the water splitting potential difference ΔG is 1.23 eV, and the photon energy E can be evaluated by the following formula:

$$E = \begin{cases} E_g, (\chi(H_2) \geq 0.2, \chi(O_2) \geq 0.6) \\ E_g + 0.2 - \chi(H_2), (\chi(H_2) < 0.2, \chi(O_2) \geq 0.6) \\ E_g + 0.6 - \chi(O_2), (\chi(H_2) \geq 0.2, \chi(O_2) < 0.6) \\ E_g + 0.8 - \chi(H_2) - \chi(O_2), (\chi(H_2) < 0.2, \chi(O_2) < 0.6) \end{cases} \quad \text{(Equation 4)}$$

The $\chi(H_2)$ and $\chi(O_2)$ indicate the overpotentials of the hydrogen and oxygen evolution reactions. The η_{sth} of the GaSSiP/arsenene and SiPGaS/arsenene vdWHs is calculated to be 30.10% and 30.57%, respectively. These values are better than those of other photocatalysts reported previously, such as arsenene/GaSe (24.91%),[42] g-C_6N_6/InP (27.32%)[56] and $WSe_2/SnSe_2$ (9.3%).[57]

Strain engineering

Strain engineering is widely acknowledged as an effective technique for tailoring the characteristics of 2D materials.[17,58] The control of band gaps via strain is firmly established in theory and experiments, driven by modified interactions and hybridizations among electronic orbitals due to structural changes in bond lengths and/or angles within a 2D lattice.[59–61] The magnitude of strain can be defined as $\varepsilon_b = (a - a_o)/a_o$,

Table 2. Deformation potential constants E_{DP} (eV), in-plane stiffness C_{2D} (Nm^{-1}), effective masses m^* (m_e) and carrier mobility μ_{2D} ($cm^2V^{-1}S^{-1}$) for the electrons and holes at 300 K in the GaSSiP/arsenene and SiPGaS/arsenene vdWHs

System	Carrier	E_{DP}	C_{2D}	m^*	μ_{2D}
Arsenene	e	3.80	49.64	0.60	1.36×10^2
	h	−3.52	49.64	0.71	1.13×10^2
SiPGaS	e	−2.51	113.45	0.42	14.55×10^2
	h	2.72	113.45	4.45	0.11×10^2
GaSSiP/arsenene	e	−3.86	159.43	0.69	3.20×10^2
	h	−5.60	159.43	0.70	1.47×10^2
SiPGaS/arsenene	e	−3.19	159.93	0.71	4.44×10^2
	h	−1.51	159.93	0.63	2.51×10^2

where a_0 and a are the in-plane lattice constants of the unstrained and strained vdWHs, respectively. Prior research has demonstrated that many 2D materials, such as graphene and transition-metal dichalcogenides, can endure strains exceeding 25%.[58,62] For instance, with a tensile strain of more than 5%, the band alignment of $MoSe_2/SnS_2$ heterostructure can be shifted from a type-I to a type-III.[63] These findings underscore the practical and effective nature of strain as a method for manipulating the electronic structures of 2D materials. In this study, we applied biaxial strain ranging from −6% to 6% to SiPGaS/arsenene-based vdWHs. From Figure S3, it is evident that biaxial strain can significantly reduce the band gap of both vdWHs, with the exception of SiPGaS/arsenene vdWH under 2% tensile strain, where the band gap initially increases and subsequently decreases moderately. Figures S4 and S5 provide additional evidence to clarify our results. Notably, the type-II band alignment remains robust over the range of applied biaxial strains depicted in Figures S6 and S7. At 6% compressive strain, the band edges of SiPGaS shift downward while those of arsenene shift upward in both GaSSiP/arsenene and SiPGaS/arsenene vdWHs, as depicted in Figures 7A and 7B. This strain-induced effect can lead to the closure of the band gap, inducing a transition from the semiconductor state to the metallic state (type-III). A prototype of a t-FET has been suggested as a promising option for digital data storage. The t-FET allows for the application of square wave pulse input voltage using pulsed alternating current field technology.[64] The flow of tunneling current between the source and drain can result in a significant or negligible electrical resistance in the semiconducting or metallic phase, respectively. This characteristic can be utilized to represent the states of "OFF (0)" or "ON (1)." For instance, Yan et al.[65] experimentally proved that a polarity switchable half-wave rectifier/bridge rectifier can be employed with a near-broken band alignment ($\Delta E_{CV} = E^2_{CBM} - E^1_{VBM}$ is in the range of E_{CV} = 0–0.2 eV; 1, 2 indicate single-layer 1 and 2 in vdWHs) utilizing a sinusoidal input voltage. Some innovative applications of SiPGaS/arsenene-based vdWHs near broken band alignment are shown in Figure 7C.

The influence of biaxial strain on the photocatalytic and optical characteristics of GaSSiP/arsenene and SiPGaS/arsenene vdWHs are inspected, as shown in Figures S8–S10. The CBE and VBE of GaSSiP/arsenene and SiPGaS/arsenene sharply shrink by applying compressive strain, while a gradual contraction is observed for tensile strain. Thus, it is clear from the results that the band edges of unstrained system have a superior photocatalytic water splitting capability over strained system. Furthermore, the change in the band gap energy leads to

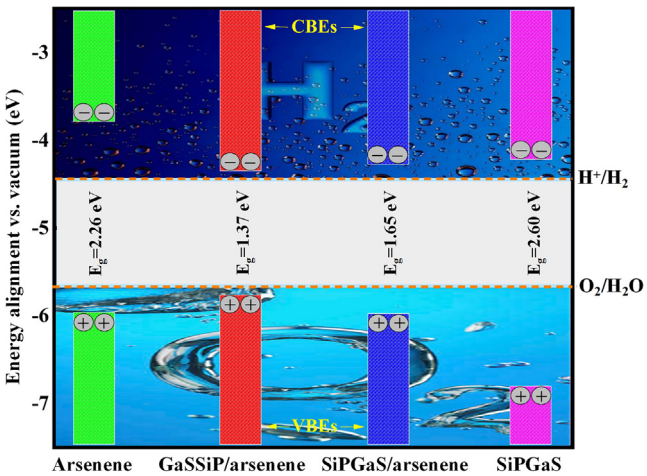

Figure 5. Calculated band edge positions with respect to the redox potentials of water using the HSE06 method

Demonstration of the band edge alignments of single-layers SiPGaS and arsenene, GaSSiP/arsenene and SiPGaS/arsenene vdWHs, as well as the reduction (H^+/H_2) and oxidation (O_2/H_2O) potentials at pH = 0.

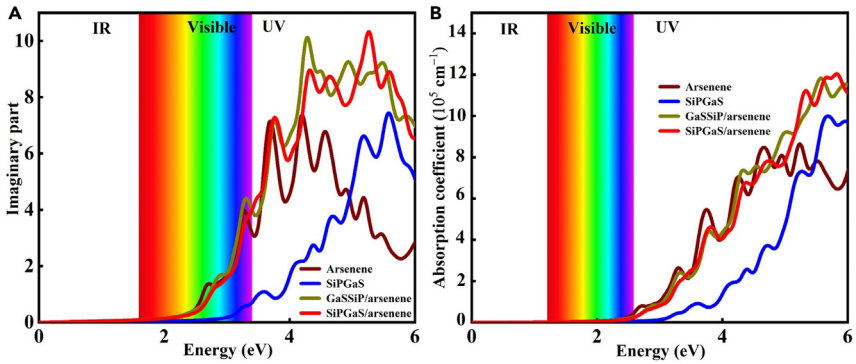

Figure 6. Calculated imaginary part of the dielectric function and absorption coefficient using the HSE06 method

(A) Imaginary part of GaSSiP/arsenene and SiPGaS/arsenene vdWHs and their corresponding single-layers.

(B) Absorption coefficient of GaSSiP/arsenene and SiPGaS/arsenene vdWHs and their corresponding single-layers.

change in the optical absorption edges of the material. On the other hand, these edges are red-shifted toward a lower energy region for the vdWHs, due to reduced band gap, as shown in Figures S9 and S10. Overall, the consequence of strain on the optical properties of materials is a pivotal factor to consider in the design and fabrication of optoelectronic devices.

Interlayer distance

Figures S11–S13 depict the influence of the interlayer distance on the electronic characteristics of GaSSiP/arsenene and SiPGaS/arsenene vdWHs. It should be noted that the interlayer couplings in vdWHs can be adjusted in experiments using scanning tunneling microscopy.[66] Figure S11 indicates that the band gap of GaSSiP/arsenene vdWH increases steadily as the interlayer distance increases, while the interlayer distance has a negligible impact on the electronic properties of SiPGaS/arsenene vdWHs. Interestingly, interlayer distance can modify the photocatalytic activity as represented in Figure S14. Increasing the interlayer distance from 3.75 Å to 4.05 Å in GaSSiP/arsenene leads the CBM and VBM favorable for straddling the redox potential of water for full water splitting at pH = 2. Similarly, in SiPGaS/arsenene vdWH, the CBM and VBM straddle the redox potential of water when the interlayer distance increases from 3.43 Å to 4.13 Å. Furthermore, variations in the interlayer distance can induce changes in the optical properties of the vdWHs, leading to reduced absorption strength and a shift of the absorption spectrum toward lower wavelengths, as shown in Figures S15 and S16. Thus, our results demonstrate that GaSSiP/arsenene and

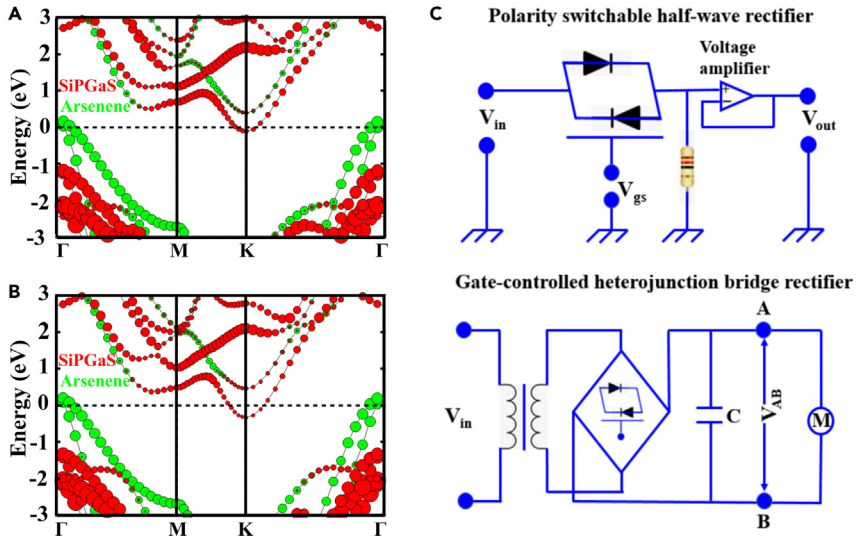

Figure 7. Calculated projected band structures and schematic illustration of field effect transistor using the HSE06 method

(A) Projected band structure of GaSSiP/arsenene vdWH at 6% compression strain (show type-III broken band alignment).

(B) Projected band structure of SiPGaS/arsenene vdWH at 6% compression strain (show type-III broken band alignment).

(C) Schematic illustration of field effect transistor. Some innovative applications of GaSSiP/arsenene and SiPGaS/arsenene vdWHs near broken band alignment (more details are explained in recent experimental work by Yan et al.[65] on 2D InSe/GeSe heterostructure).

SiPGaS/arsenene are potential candidates for harvesting maximum portion of the solar spectrum and for use as photocatalysts for full water splitting.

Outlook

We have studied photocatalytic and optical properties of the SiPGaS/arsenene-based vdWHs. Notably, the SiPGaS/arsenene-based vdWHs exhibit a type-II band alignment, effectively facilitating the spatial separation of photo-induced charge carriers, which is crucial for the design of photovoltaic devices. For this, we expect a focused investigation into the excitonic properties of the vdWHs will also be required, due to their reduced dielectric screening and quantum confinement effects. As 2D layered materials are self-passivated, individual single-layers interact only weakly via vdW forces. In case of semiconducting 2D materials, such as single-layers of transition-metal dichalcogenides and those involved in this work, due to such weak interlayer coupling, the single-particle electronic states close to the bandgap can be considered to be largely localized within the individual layers. One can thus directly examine the relative energy difference, or band alignment of electronic band extrema (i.e., CBM and VBM), without having to take into account the lattice matching or epitaxy of a vdWH. However, since the electrons of the individual layers still extend out of the plane, different electronic states can couple to one another in ways that are not possible in other systems. As a result, the properties of a vdWH is defined not only by the constituent monolayers, but also by the stacking sequence and relative crystallographic alignment of the layers. In particular, the latter, which concerns the atomic registry between constituent layers, has now been identified as a powerful approach to tune the interlayer coupling.[67,68] Essentially, this approach exploits the periodic potential modulation in moiré lattice of twisted homo-bilayer or lattice-mismatched crystals to control band structure and even induce unconventional correlated or topological phenomena. As such, we anticipate this to serve as a strong motivation for extending the present study.

Conclusion

By means of *ab initio* computation schemes, we have undertaken a comprehensive investigation into the electronic, photocatalytic, and optical characteristics of SiPGaS/arsenene-based vdWHs. Using PBE/HSE06 functional, we found that GaSSiP/arsenene- and SiPGaS/arsenene vdWHs possess indirect band gaps of 0.79/1.37 eV and 1.00/1.65 eV, respectively. The projected band structure and PDOS reveal the CBM and VBM of both vdWHs to originate from different layers, effectively mitigating the recombination of photoexcited charge carriers. Notably, the vdWHs exhibit prominent absorption peaks across the whole visible region of the solar spectrum, while their band edge positions render them suitable for full water splitting at pH = 0. We further demonstrated that applying 6% compressive strain can induce a transition in the band alignment of these vdWHs from type-II to type-III, thereby rendering them applicable in the context of t-FET applications. Increasing the interlayer distance of the SiPGaS/arsenene-based vdWHs can enhance the water redox potentials at pH = 2, which is crucial for water splitting reactions in acidic environments. The findings of this study can serve as practical guidelines for leveraging these materials in a wide range of optoelectronic and photocatalytic applications.

Limitations of the study

The optical properties are calculated based on the HSE06 method. However, this method may not capture excitonic effects and higher-energy excited states accurately. GW-BSE method can be used for accurate optical calculations.

STAR★METHODS

Detailed methods are provided in the online version of this paper and include the following:

- KEY RESOURCES TABLE
- RESOURCE AVAILABILITY
  - Lead contact
  - Materials availability
  - Data and code availability
- METHOD DETAILS
  - Calculation method

SUPPLEMENTAL INFORMATION

Supplemental information can be found online at https://doi.org/10.1016/j.isci.2023.108025.

ACKNOWLEDGMENTS

This work is supported by the Natural Science Foundation of China (12274343), the Natural Science Foundation of Shaanxi Province (No. 2022JM-030), the Natural Science Foundation of Chongqing (cstc2021jcyj-msxmX0740), and the Basic Research Program of Taicang (TC2022JC15).

AUTHOR CONTRIBUTIONS

A.A.: Conceptualization, Methodology, Writing–original draft. I.S.: Formal analysis, Validation, review and editing. I.A.: Validation, Review and editing. B.L.: Review and editing. H.Z.: Review and editing. P.K.J.W.: Writing – review and editing, Supervision, Resources. W.Z.: Investigation, Supervision, Resources.

DECLARATION OF INTERESTS

The authors declare no competing interests.

Received: June 9, 2023
Revised: September 5, 2023
Accepted: September 19, 2023
Published: September 23, 2023

REFERENCES

1. Dresselhaus, M.S., and Thomas, I.L. (2001). Alternative energy technologies. Nature *414*, 332–337.
2. Tachibana, Y., Vayssieres, L., and Durrant, J.R. (2012). Artificial photosynthesis for solar water-splitting. Nat. Photonics *6*, 511–518.
3. Yu, H., Dai, M., Zhang, J., Chen, W., Jin, Q., Wang, S., and He, Z. (2023). Interface Engineering in 2D/2D Heterogeneous Photocatalysts. Small *19*, 2205767.
4. Bi, Y., Yang, Y., Shi, X.-L., Feng, L., Hou, X., Ye, X., Zhang, L., Suo, G., Lu, S., and Chen, Z.-G. (2021). Full-spectrum responsive photocatalytic activity via non-noble metal Bi decorated mulberry-like $BiVO_4$. J. Mater. Sci. Technol. *83*, 102–112.
5. Zou, X., Yang, Y., Chen, H., Shi, X.-L., Suo, G., Ye, X., Zhang, L., Hou, X., Feng, L., and Chen, Z.-G. (2020). Tuning wall thickness of TiO_2 microtubes for an enhanced photocatalytic activity with thickness-dependent charge separation efficiency. J. Colloid Interface Sci. *579*, 463–469.
6. Qu, Y., and Duan, X. (2013). Progress, challenge and perspective of heterogeneous photocatalysts. Chem. Soc. Rev. *42*, 2568–2580.
7. Jang, J.S., Kim, H.G., and Lee, J.S. (2012). Heterojunction semiconductors: A strategy to develop efficient photocatalytic materials for visible light water splitting. Catal. Today *185*, 270–277.
8. Ge, J., Zhang, Y., Heo, Y.-J., and Park, S.-J. (2019). Advanced Design and Synthesis of Composite Photocatalysts for the Remediation of Wastewater: A Review. Catalysts *9*, 122.
9. Zhuang, H.L., and Hennig, R.G. (2013). Single-Layer Group-III Monochalcogenide Photocatalysts for Water Splitting. Chem. Mater. *25*, 3232–3238.
10. Mak, K.F., and Shan, J. (2016). Photonics and optoelectronics of 2D semiconductor transition metal dichalcogenides. Nat. Photonics *10*, 216–226.
11. Lim, E.L., and Wei, Z. (2023). Can two-dimensional graphdiyne-based materials be novel materials for perovskite solar cell applications? Mater. Futures *2*, 027501.
12. Kang, S., Eshete, Y.A., Lee, S., Won, D., Im, S., Lee, S., Cho, S., and Yang, H. (2022). Bandgap modulation in the two-dimensional core-shell-structured monolayers of WS_2. iScience *25*, 103563.
13. Cui, Z., and Wu, H. (2023). Metal atoms adsorbed Ga_2O_3 monolayer: As a potential application in optoelectronic devices. Micro Nanostruct. *180*, 207613.
14. Liu, W., Wang, S., Lu, W., Cheng, Z., and Jiang, N. (2019). Hybrid spintronic materials: Growth, structure and properties. AAPS PharmSciTech *21*, 27–105.
15. Zhang, W., Wong, P.K.J., Jiang, S., Chen, Q., Huang, W., and Wee, A.T.S. (2021). Integrating spin-based technologies with atomically controlled van der Waals interfaces. Mater. Today *51*, 350–364.
16. Zhang, W., Wong, P.K.J., Zhu, R., and Wee, A.T.S. (2019). Van der Waals magnets: Wonder building blocks for two-dimensional spintronics? InfoMat *1*, 479–495.
17. You, J.-Y. (2023). Strain induced metal-semiconductor transition in two-dimensional topological half metals. iScience *26*, 106312.
18. Lu, Q., Yu, Y., Ma, Q., Chen, B., and Zhang, H. (2016). 2D Transition-Metal-Dichalcogenide-Nanosheet-Based Composites for Photocatalytic and Electrocatalytic Hydrogen Evolution Reactions. Adv. Mater. *28*, 1917–1933.
19. Obeid, M.M., Bafekry, A., Ur Rehman, S., and Nguyen, C.V. (2020). A type-II GaSe/HfS_2 van der Waals heterostructure as promising photocatalyst with high carrier mobility. Appl. Surf. Sci. *534*, 147607.
20. Lin, L., Pang, D., Shi, P., Yan, L., Lou, M., Chen, R., Chen, Y., Wang, Y., and Zhang, Z. (2022). Strain facilitated small gas molecules sensing properties on Au doped $SnSe_2$ monolayer. Int. J. Hydrogen Energy *47*, 14361–14370.
21. Huang, G., Zhang, G., Gao, Z., Cao, J., Li, D., Yun, H., and Zeng, T. (2019). Enhanced visible-light-driven photocatalytic activity of $BiFeO_3$ via electric-field control of spontaneous polarization. J. Alloys Compd. *783*, 943–951.
22. Bi, Y., Yang, Y., Shi, X.-L., Feng, L., Hou, X., Ye, X., Zhang, L., Suo, G., Chen, J., and Chen, Z.-G. (2021). Bi_2O_3/$BiVO_4$/graphene oxide van der Waals heterostructures with enhanced photocatalytic activity toward oxygen generation. J. Colloid Interface Sci. *593*, 196–203.
23. Su, Q., Li, Y., Hu, R., Song, F., Liu, S., Guo, C., Zhu, S., Liu, W., and Pan, J. (2020). Heterojunction Photocatalysts Based on 2D Materials: The Role of Configuration. Sustain. Syst. *4*, 2000130.
24. Cui, Z., Ren, K., Zhao, Y., Wang, X., Shu, H., Yu, J., Tang, W., and Sun, M. (2019). Electronic and optical properties of van der Waals heterostructures of g-GaN and transition metal dichalcogenides. Appl. Surf. Sci. *492*, 513–519.
25. Shahid, I., Ali, A., Zhang, J.-M., Muhammad, I., Ahmad, I., and Kabir, F. (2021). Two dimensional MoSSe/BSe vdW heterostructures as potential photocatalysts for water splitting with high carrier mobilities. Int. J. Hydrogen Energy *46*, 14247–14258.
26. Liu, J., Li, Z., Zhang, X., and Lu, G. (2021). Unraveling energy and charge transfer in type-II van der Waals heterostructures. npj Comput. Mater. *7*, 191.
27. Cao, M., Ni, L., Wang, Z., Liu, J., Tian, Y., Zhang, Y., Wei, X., Guo, T., Fan, J., and Duan, L. (2021). DFT investigation on direct Z-scheme photocatalyst for overall water splitting: $MoTe_2$/BAs van der Waals heterostructure. Appl. Surf. Sci. *551*, 149364.
28. Hu, L., Yi, W., Rao, T., Tang, J., Hu, C., Yin, H., Hao, H., Zhang, L., Li, C., and Li, T. (2020). Two-dimensional type-II g-C_3N_4/SiP–GaS heterojunctions as water splitting photocatalysts: first-principles predictions. Phys. Chem. Chem. Phys. *22*, 15649–15657.
29. Shahid, I., Ahmad, S., Shehzad, N., Yao, S., Nguyen, C.V., Zhang, L., and Zhou, Z. (2020). Electronic and photocatalytic performance of boron phosphide-blue phosphorene vdW heterostructures. Appl. Surf. Sci. *523*, 146483.
30. Giampietri, A., Drera, G., and Sangaletti, L. (2017). Band Alignment at Heteroepitaxial Perovskite Oxide Interfaces. Experiments, Methods, and Perspectives. Adv. Mater. Interfac. *4*, 1700144.
31. Shehzad, N., Saeed, S., Shahid, I., Khan, I., Saeed, I., Zapien, J.A., and Zhang, L. (2022). Two-dimensional van der Waals heterostructures (vdWHs) with band alignment transformation in multi-functional devices. RSC Adv. *12*, 31456–31465.
32. Nakamura, S., Senoh, M., Iwasa, N., and Shin-ichi Nagahama, S.i.N. (1995). High-Brightness InGaN Blue, Green and Yellow Light-Emitting Diodes with Quantum Well Structures. Jpn. J. Appl. Phys. *34*, L797.
33. Özçelik, V.O., Azadani, J.G., Yang, C., Koester, S.J., and Low, T. (2016). Band alignment of two-dimensional semiconductors for designing heterostructures with momentum space matching. Phys. Rev. B *94*, 35125.
34. Ahmad, I., Shahid, I., Ali, A., Ruan, Z., Yan, C., Ali, J., Gao, L., and Cai, J. (2022). Two dimensional Janus SGaInSe(SeGaInS)/$PtSe_2$ van der Waals heterostructures for optoelectronic and photocatalytic water

splitting applications. Int. J. Hydrogen Energy *47*, 28833–28844.
35. Lin, J.-H., Zhang, H., Cheng, X.-L., and Miyamoto, Y. (2017). Single-layer group IV-V and group V-IV-III-VI semiconductors: Structural stability, electronic structures, optical properties, and photocatalysis. Phys. Rev. B *96*, 035438.
36. Kamal, C., and Ezawa, M. (2015). Arsenene: Two-dimensional buckled and puckered honeycomb arsenic systems. Phys. Rev. B *91*, 085423.
37. Zhang, S., Xie, M., Li, F., Yan, Z., Li, Y., Kan, E., Liu, W., Chen, Z., and Zeng, H. (2016). Semiconducting Group 15 Monolayers: A Broad Range of Band Gaps and High Carrier Mobilities. Angew. Chem. Int. Ed. Engl. *55*, 1666–1669.
38. Hu, P., Wang, L., Yoon, M., Zhang, J., Feng, W., Wang, X., Wen, Z., Idrobo, J.C., Miyamoto, Y., Geohegan, D.B., and Xiao, K. (2013). Highly Responsive Ultrathin GaS Nanosheet Photodetectors on Rigid and Flexible Substrates. Nano Lett. *13*, 1649–1654.
39. Pumera, M., and Sofer, Z. (2017). 2D Monoelemental Arsenene, Antimonene, and Bismuthene: Beyond Black Phosphorus. Adv. Mater. *29*, 1605299.
40. Chai, J., Wang, Z., and Li, Y. (2020). Investigation of the mechanism of overall water splitting in UV-visible and infrared regions with SnC/arsenene vdW heterostructures in different configurations. Phys. Chem. Chem. Phys. *22*, 1045–1052.
41. Yang, J., Wei, X., Zhang, J., Huang, Y., Zhu, G., Han, S., and Wang, Z. (2022). Two-dimensional g-C6N6/SiP-GaS van der Waals heterojunction for overall water splitting under visible light. Int. J. Hydrogen Energy *47*, 16014–16024.
42. Li, J., Huang, Z., Ke, W., Yu, J., Ren, K., and Dong, Z. (2021). High solar-to-hydrogen efficiency in Arsenene/GaX (X = S, Se) van der Waals heterostructure for photocatalytic water splitting. J. Alloys Compd. *866*, 158774.
43. Chen, S., Tan, H.y., Wu, Z.h., Sun, C.p., He, J.x., Li, X.c., and Shao, M. (2014). Study on the separation mechanisms of photogenerated electrons and holes for composite photocatalysts g-C3N_4-WO_3. Eur. J. Radiol. *83*, 564–570.
44. Qiao, P., Xia, J., Li, X., Ru, F., Liu, P., Tian, L., Jiang, X., Lin, Z., Chen, X., and Meng, X.-M. (2022). Edge-Assisted Epitaxy of 2D $TaSe_2$-$MoSe_2$ Metal–Semiconductor Heterostructures and Application to Schottky Diodes. Adv. Funct. Mater. *32*, 2201449.
45. Wang, B.-J., Li, X.-H., Zhao, R., Cai, X.-L., Yu, W.-Y., Li, W.-B., Liu, Z.-S., Zhang, L.-W., and Ke, S.-H. (2018). Electronic structures and enhanced photocatalytic properties of blue phosphorene/BSe van der Waals heterostructures. J. Mater. Chem. A *6*, 8923–8929.
46. Li, C., Xu, Y., Sheng, W., Yin, W.-J., Nie, G.-Z., and Ao, Z. (2020). A promising blue phosphorene/C_2N van der Waals type-II heterojunction as a solar photocatalyst: a first-principles study. Phys. Chem. Chem. Phys. *22*, 615–623.
47. Wang, G., Geng, L., Tang, W., Wang, B., Zhao, W., Zhang, W., Yuan, B., Yuan, H., and Zhou, T. (2020). Two dimensional CdS/ZnO type-II heterostructure used for photocatalytic water-splitting. Nanotechnology *31*, 485701.
48. Han, S., Li, Y., Chai, J., and Wang, Z. (2020). Study of the GaAs/SiH van der Waals type-II heterostructure: a high efficiency photocatalyst promoted by a built-in electric field. Phys. Chem. Chem. Phys. *22*, 8565–8571.
49. Jia, M., Ren, F., Chen, X., Han, W., Jin, C., Peng, C., and Wang, B. (2023). Polarization and built-in electric field improve the photocatalytic overall water splitting efficiency of C_2N/ZnSe heterostructures. Int. J. Hydrogen Energy *48*, 19554–19563.
50. Zhang, X., Zhao, X., Wu, D., Jing, Y., and Zhou, Z. (2016). $MnPSe_3$ Monolayer: A Promising 2D Visible-Light Photohydrolytic Catalyst with High Carrier Mobility. Adv. Sci. *3*, 1600062.
51. Ahmad, S., Sohail, K., Chen, L., Xu, H., Din, H.U., and Zhou, Z. (2023). Type-II van der Waals heterostructures of GeC, ZnO and Al_2SO monolayers for promising optoelectronic and photocatalytic applications. Int. J. Hydrogen Energy *48*, 25354–25365.
52. Wang, B.-J., Li, X.-H., Cai, X.-L., Yu, W.-Y., Zhang, L.-W., Zhao, R.-Q., and Ke, S.-H. (2018). Blue Phosphorus/$Mg(OH)_2$ van der Waals Heterostructures as Promising Visible-Light Photocatalysts for Water Splitting. J. Phys. Chem. C *122*, 7075–7080.
53. Ren, K., Yu, J., and Tang, W. (2020). Two-dimensional ZnO/BSe van der waals heterostructure used as a promising photocatalyst for water splitting: A DFT study. J. Alloys Compd. *812*, 152049.
54. Shu, H. (2021). Adjustable electro-optical properties of novel graphene-like SiC_2 via strain engineering. Appl. Surf. Sci. *559*, 149956.
55. Kolås, T., Røyset, A., Grandcolas, M., Cate, M.t., and Lacau, A. (2019). Cool coatings with high near infrared transmittance for coil coated aluminium. Sol. Energy Mater. Sol. Cells *196*, 94–104.
56. Wenna, H., Xuefeng, C., Minglei, J., Fengzhu, R., Chengxiao, P., Haigang, Y., Qinfen, G., Bing, W., and Huabing, Y. (2022). A direct Z-scheme g-C_6N_6/InP van der Waals heterostructure: a promising photocatalyst for high-efficiency overall water splitting. J. Phys. D Appl. Phys. *55*, 264001.
57. Fan, Y., Wang, J., and Zhao, M. (2019). Spontaneous full photocatalytic water splitting on 2D $MoSe_2$/$SnSe_2$ and WSe_2/$SnSe_2$ vdW heterostructures. Nanoscale *11*, 14836–14843.
58. Kim, K.S., Zhao, Y., Jang, H., Lee, S.Y., Kim, J.M., Kim, K.S., Ahn, J.-H., Kim, P., Choi, J.-Y., and Hong, B.H. (2009). Large-scale pattern growth of graphene films for stretchable transparent electrodes. Nature *457*, 706–710.
59. Quan, S., Zhang, Y., and Chen, W. (2022). Strain effects in the electron orbital coupling and electric structure of graphene. Phys. Chem. Chem. Phys. *24*, 23929–23935.
60. Johari, P., and Shenoy, V.B. (2012). Tuning the Electronic Properties of Semiconducting Transition Metal Dichalcogenides by Applying Mechanical Strains. ACS Nano *6*, 5449–5456.
61. Ahn, G.H., Amani, M., Rasool, H., Lien, D.-H., Mastandrea, J.P., Ager Iii, J.W., Dubey, M., Chrzan, D.C., Minor, A.M., and Javey, A. (2017). Strain-engineered growth of two-dimensional materials. Nat. Commun. *8*, 608.
62. Feng, J., Qian, X., Huang, C.-W., and Li, J. (2012). Strain-engineered artificial atom as a broad-spectrum solar energy funnel. Nat. Photonics *6*, 866–872.
63. Zhao, X., Wang, M., Niu, W., Zhang, H., Wang, T., and Dai, X. (2021). Tunable band alignments and optical properties in vertical heterojunctions of SnS_2 and $MoSe_2$. Solid State Commun. *323*, 114103.
64. Vicario, C., Monoszlai, B., and Hauri, C.P. (2014). GV/m Single-Cycle Terahertz Fields from a Laser-Driven Large-Size Partitioned Organic Crystal. Phys. Rev. Lett. *112*, 213901.
65. Yan, Y., Li, S., Du, J., Yang, H., Wang, X., Song, X., Li, L., Li, X., Xia, C., Liu, Y., et al. (2021). Reversible Half Wave Rectifier Based on 2D InSe/GeSe Heterostructure with Near-Broken Band Alignment. Adv. Sci. *8*, 1903252.
66. Yankowitz, M., Watanabe, K., Taniguchi, T., San-Jose, P., and LeRoy, B.J. (2016). Pressure-induced commensurate stacking of graphene on boron nitride. Nat. Commun. *7*, 13168.
67. Novoselov, K.S., Mishchenko, A., Carvalho, A., and Castro Neto, A.H. (2016). 2D materials and van der Waals heterostructures. Science *353*, 461.
68. Kennes, D.M., Claassen, M., Xian, L., Georges, A., Millis, A.J., Hone, J., Dean, C.R., Basov, D.N., Pasupathy, A.N., and Rubio, A. (2021). Moiré heterostructures as a condensed-matter quantum simulator. Nat. Phys. *17*, 155–163.
69. Kresse, G., and Furthmüller, J. (1996). Efficient iterative schemes for ab initio total-energy calculations using a plane-wave basis set. Phys. Rev. B *54*, 11169–11186.
70. Blöchl, P. (1994). Projector augmented-wave method. Phys. Rev. B *50*, 17953–17979.
71. Kresse, G., and Joubert, D. (1999). From ultrasoft pseudopotentials to the projector augmented-wave method. Phys. Rev. B *59*, 1758–1775.
72. Wahab, T., Wang, Y., and Cammarata, A. (2023). A first principles study of structural and optoelectronic properties and photocatalytic performance of GeC–MX_2 (M = Mo and W; X = S and Se) van der Waals heterostructures. Phys. Chem. Chem. Phys. *25*, 11169–11175.
73. Cui, Z., Yang, K., Shen, Y., Yuan, Z., Dong, Y., Yuan, P., and Li, E. (2023). Toxic gas molecules adsorbed on intrinsic and defective WS_2: gas sensing and detection. Appl. Surf. Sci. *613*, 155978.
74. Paier, J., Marsman, M., Hummer, K., Kresse, G., Gerber, I.C., and Angyán, J.G. (2006). Screened hybrid density functionals applied to solids. J. Chem. Phys. *124*, 154709.
75. Grimme, S., Antony, J., Ehrlich, S., and Krieg, H. (2010). A consistent and accurate ab initio parametrization of density functional dispersion correction (DFT-D) for the 94 elements H-Pu. J. Chem. Phys. *132*, 154104.
76. Togo, A., and Tanaka, I. (2015). First principles phonon calculations in materials science. Scripta Mater. *108*, 1–5.
77. Nosé, S. (1984). A unified formulation of the constant temperature molecular dynamics. J. Chem. Phys. *81*, 511–519.

STAR★METHODS

KEY RESOURCES TABLE

REAGENT or RESOURCE	SOURCE	IDENTIFIER
Software		
VASP 5.4.4	Kresse and Furthmüller	https://www.vasp.at
PHONOPY	Togo and Tanaka	phonopy.github.io/phonopy/
VESTA	Momma and Izumi	http://jp-minerals.org/vesta/

RESOURCE AVAILABILITY

Lead contact

Further information and requests for resources should be directed to the lead contact, Ping Kwan Johnny Wong (pingkwanj.wong@nwpu.edu.cn).

Materials availability

This study did not generate new unique reagents.

Data and code availability

- The published article includes all datasets generated or analyzed during this study.
- This study did not generate new code.
- Any additional information required to reanalyze the data reported in this paper is available from the lead contact upon request.

METHOD DETAILS

Calculation method

We performed first-principles computations on SiPGaS/arsenene-based vdWHs and their parent single-layers, using the Vienna ab initio simulation package.[69] The exchange-correlation function was treated through the generalized gradient approximation within the scheme of the Perdew–Burke–Ernzerhof (GGA-PBE).[70] The projector-augmented wave (PAW) potentials were used to describe the ion-electron interaction.[71] The cutoff value was set to 520 eV for the plane wave expansion of the wave functions. To avoid any possible interactions between adjacent layers, a vacuum length of 25 Å was introduced in the z-axis. During structural optimization, the force and energy converged to 10^{-5} eV and 0.01 eVÅ^{-1}, respectively. In addition, we have also set an energy convergence criterion of 10^{-6} eV/Å and performed calculations on SiPGaS/arsenene-based vdWHs. Our findings indicated that there is negligible disparity in the total energies among these systems. A convergence criterion of 10^{-5} eV/Å is enough for accurately estimating the ground state properties of the systems.[72,73]The hybrid functional Heyd-Scuseria-Ernzerhof-06 (HSE06)[74] was included to accurately calculate the electronic band gap of the semiconductor. The DFT-D3 approach[75] with the Grimme-vdW correction was used to treat the vdW interaction between the adjacent layers. A Monkhorst–Pack k-points mesh with a size of 14×14×1 was employed for both the geometry optimization and HSE06 calculations. To evaluate the dynamical stability, we calculated their phonon dispersion by using the PHONOPY code.[76] To establish thermal stability on the vdWHs, ab-initio molecular dynamic (AIMD) simulations[77] were performed at 500 K, with a time step of 2.0 fs for 5 ps. For the phonon and AIMD calculations, we employed supercells of vdWHs with sizes of 4×4×1 and 3×3×1, respectively.